

Preliminary Design Review

In fulfillment of the NASA University Student Launch Initiative requirements



University of Illinois at Urbana-Champaign

Illinois Space Society (ISS)

104 S Wright Street
Urbana, Illinois 61801

Todo list

Add administrative and financial officers	3
Draft team-derived requirements	14
Expand on deployment requirements (robustness, rapidity) and ground proximity considerations . . .	16
Expand on descent phase, including trade-offs between guidance algorithms ((N)MPC, GPC) and waypoint tracking vs. visual guidance at close proximity (CV).	16
Expand on loiter phase, highlighting energy efficiency and data acquisition (feature detection and path planning) during idle phase. Also detail what safety features must be incorporated into this phase (geofencing, no-fly zones have to default back to loiter).	16
Expand on final approach and landing phase, including close-quarters operations and the role of computer vision in detecting the landing site, as well as the accuracy and terminal touch down conditions (velocity, attitude). Explain touch-and-go maneuvers in case of failed landing attempt. . .	16
Expand on retrieval protocol, including claw operations and validation of claw contents. Explain the details on distancing and safe idle mode after retrieval, as well as shutdown/hibernation routines.	16
Add NAR High Power Rocketry Code to appendix	29
Add sec. on hazardous operations	29
Add sec. on risk mitigation	29
Add sec. on hazardous materials	29

List of Figures

2.1 VFR aeronautical chart of the Hazel Green, AL area	13
--	----

List of Tables

4.1	Simulation parameters	24
4.2	Maximum state deviation values for use in the $\bar{\mathbf{Q}}_1$ matrix in the Linear Quadratic Regulator (LQR) routine	25
6.1	Level of risk and member requirements	31

ACKNOWLEDGEMENT

<u>AREA</u>	<u>NAME/FUNCTION</u>	<u>SUBTEAM</u>
Parts I, II, VI	H. El-Kebir <i>Team Lead</i>	—
Part III <i>Vehicle configuration</i>	G. Petrov <i>Subteam Lead</i>	Structures & Recovery
Part III <i>Avionics</i>	M. Bourla <i>Subteam Lead</i>	Avionics
Part III <i>Flight simulations</i>	R. Filipiuk <i>Subteam Lead</i>	Flight Dynamics
Part IV <i>Payload configuration</i>	K. Tochihara <i>Project Manager</i>	Payload
Part IV <i>Control systems</i>	A. Yaraneri <i>Chief Engineer</i>	Payload
Part V	Z. Essmyer <i>Ancillary Subteam Lead</i>	Ancillary

HE: Add administrative and financial officers

It is requested that any organizations having specific comments in their area of responsibility contact the individual(s) listed above.

Acronyms

CDR Critical Design Review. 7

CFD Computational Fluid Dynamics. 19

CM Center of Mass. 18

CONOPS Concept of Operations. 7

EIA Environmental Impact Assessment. 7

FAA Federal Aviation Authority. 12, 13, 15

FMEA Failure Modes and Effects Analysis. 7

ISS Illinois Space Society. 7

LOS Line of Sight. 13, 15

LQR Linear Quadratic Regulator. 2, 6, 25

MIMO Multiple Input Multiple Output. 25

MoI Moment of Inertia. 18

NAR National Association of Rocketry. 12

PDR Preliminary Design Review. 7

PHA Personnel Hazard Analysis. 7

RMS Root Mean Square. 25

RSO Range Safety Officer. 13, 16

ToI Tensor of Inertia. 18, 19

UAV Unmanned Aerial Vehicle. 13–19, 24, 25

VFR Visual Flight Rules. 13

ZOH Zero-order Hold. 23

Contents

List of Figures	1
List of Tables	2
Acknowledgement	3
Glossary	4
Contents	5
1 Preface	7
I Summary	8
II Changes	9
III Launch Vehicle	10
IV Payload	11
2 Payload Deployment	12
2.1 Requirements	12
2.1.1 Top-level requirements	12
2.1.2 Team-derived requirements	14
2.2 Means of Securement	14
2.3 Means of Deployment	14
2.4 Leading Design	14
3 Operational Protocols	15
3.1 Transit & Deployment	15
3.2 Descent	16
3.3 Loiter	16
3.4 Landing	16
3.5 Retrieval	16

<i>CONTENTS</i>	6
4 Quadrotor Dynamic Model	17
4.1 Coordinate Systems	17
4.1.1 Coordinate Transformation	18
4.2 Dynamic Model	18
4.2.1 Nonlinear state space model	20
4.2.2 Linearized state space model	21
4.2.3 Discretization	23
4.3 Simulation	23
4.4 Controller Design	24
4.4.1 LQR Tuning	25
V Safety	27
5 Safety Plan Overview	28
5.1 Emergency Preparedness	28
5.2 Incident Reporting	28
5.3 Equipment Training	29
5.4 NAR/TRA Procedures	29
6 Risk Assessment Overview	31
VI Project Plan	32
Bibliography	33

Chapter 1

Preface

This document (ISS/USLI-PDR) serves as the [Preliminary Design Review \(PDR\)](#) for the University of Illinois at Urbana-Champaign University Student Launch Initiative team, [Illinois Space Society \(ISS\)](#). The content of this report will chiefly focus on the changes since the original proposal, developments in design and underlying justifications, as well as overall prospects and plans towards the [Critical Design Review \(CDR\)](#). In particular, the launch vehicle design is detailed with reference to the pertinent vehicle requirements, providing an overview of its subsystems, interfaces, and manufacturing methods. Safety considerations are addressed through a multitude of simulations, as well as a qualitative [Failure Modes and Effects Analysis \(FMEA\)](#) and [Environmental Impact Assessment \(EIA\)](#). Following this discussion, the payload requirements and preliminary design of both the airframe and sample retrieval mechanism are presented, culminating in the presentation of a detailed [Concept of Operations \(CONOPS\)](#). The payload-launch vehicle interface as well as the aerial deployment mechanism are discussed, giving rise to a detailed safety analysis. As part of the safety analysis, in addition to a comprehensive [FMEA](#), a [Personnel Hazard Analysis \(PHA\)](#) is presented. Any hazardous activities will be identified as part of this discussion, including any foreseeable contingencies and mitigation procedures. Finally, a project plan is presented, including a project timeline (Gantt chart), bill of materials, list of funding sources and mitigation procedures in case of delays.

This report is composed of six parts, in which each part builds forth upon the previous. These parts are:

- I Summary
- II Changes
- III Launch Vehicle
- IV Payload
- V Safety
- VI Project Plan

Each of these parts describes in due detail the developments and rationale behind the launch vehicle and payload design, as well as the overall implementation.

DISCLAIMER: While the authors have gone through great lengths to ensure the validity of all data presented in this document, all responsibility is assumed for any inconsistencies presented as part of this work.

Part I

Summary

Part II

Changes

Part III

Launch Vehicle

Part IV

Payload

Chapter 2

Payload Deployment

During the boost, coast, and the majority of the launch vehicle's flight, the payload will remain idle and securely fixed in the payload bay. This chapter will detail the means of securement and deployment of the payload, as well as a trade-off between the various means that have been considered to arrive at the leading design.

This chapter will be structured as follows: Sec. 2.1 details the requirements the payload is to satisfy given the overall mission and top-level requirements, followed by a trade-off study regarding the means of securement in Sec. 2.2, as well as the possible deployment modes in Sec. 2.3. Finally, the leading design is presented in Sec. 2.4 in reference to the foregoing trade-off studies.

2.1 Requirements

This section details the various requirements to which the payload deployment scheme must abide. Specifically, two forms of requirements are identified: top-level requirements and team-derived requirements. The first are requirements either imposed by the competition, or legislation that is in effect at the time of launch and operations. The second form of requirements pertain to what the team perceives to be of importance in assuring mission success and robustness.

2.1.1 Top-level requirements

The top-level requirements for the payload deployment are outlined in Secs. 4.3–4 of [1], reading as follows:

4.4. Lunar Ice Sample Recovery Mission Requirements

- 4.3.1. Teams must abide by all [Federal Aviation Authority \(FAA\)](#) and [National Association of Rocketry \(NAR\)](#) rules and regulations.
- 4.3.2. Black Powder and/or similar energetics are only permitted for deployment of in-flight recovery systems. Any ground deployments must utilize mechanical systems.
- 4.3.3. Any part of the payload or vehicle that is designed to be deployed, whether on the ground or in the air, must be fully retained until it is deployed as designed.
 - 4.3.7.1. A mechanical retention system will be designed to prohibit premature deployment.
 - 4.3.7.2. The retention system will be robust enough to successfully endure flight forces experienced during both typical and atypical flights.
 - 4.3.7.3. The designed system will be fail-safe.
 - 4.3.7.4. Exclusive use of shear pins will not meet this requirement.

4.6. Special Requirements for UAVs and Jettisoned Payloads

- 4.4.1. Any experiment element that is jettisoned during the recovery phase will receive real-time Range Safety Officer (RSO) permission prior to initiating the jettison event.
 - 4.4.2. Unmanned Aerial Vehicle (UAV) payloads, if designed to be deployed during descent, will be tethered to the vehicle with a remotely controlled release mechanism until the RSO has given permission to release the UAV.
 - 4.4.3. Teams flying UAVs will abide by all applicable FAA regulations, including the FAA's Special Rule for Model Aircraft (Public Law 112-95 Section 336; see <https://www.faa.gov/uas/faqs>).
 - 4.4.4. Any UAV weighing more than .55 lbs. will be registered with the FAA and the registration number marked on the vehicle.

In addition, by [FAA](#) regulations [2], the [UAV](#) may only be operated below 400 ft in [Line of Sight \(LOS\)](#)¹. From the [FAA Reauthorization Act of 2018](#), the following pertinent regulations may be found. The [UAV](#) must have a gross weight under 4.4 lbm, and must be operated:

- (i) within or beyond visual LOS of the operator;
 - (ii) less than 400 ft above ground;
 - (iii) during daylight conditions;
 - (iv) within Class G airspace; and
 - (v) outside of 5 statute miles from any airport, heliport, seaplane base, spaceport, or other location with aviation activities.

As a supplement to these regulations, an aeronautical chart of the surroundings of the launch site (Bragg Farms, Hazel Green, AL) is given in Fig. 2.1.

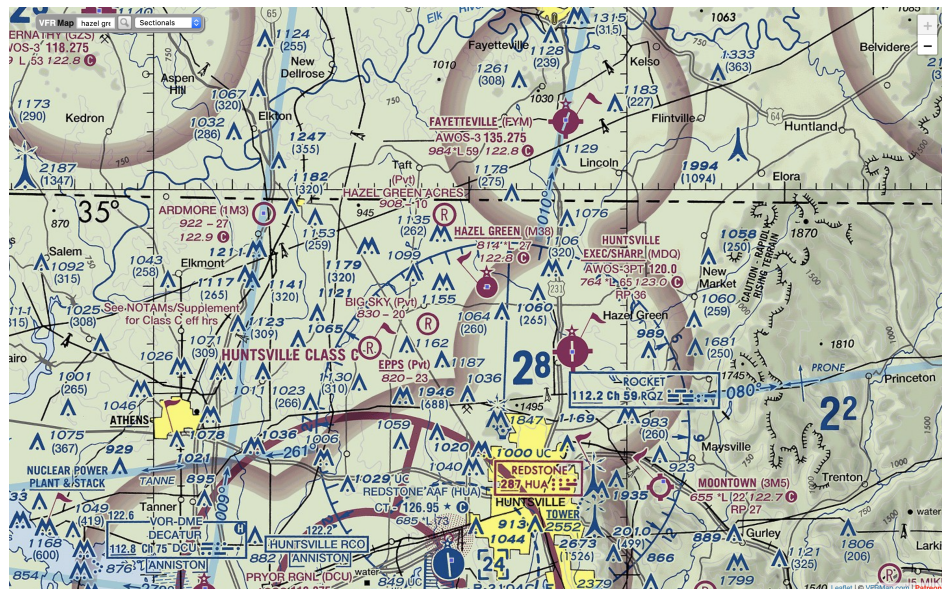


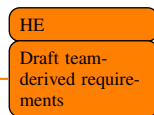
Figure 2.1: Visual Flight Rules (VFR) aeronautical chart of the Hazel Green, AL area. Adapted from [VFRMap.com](#)

¹FAA Reauthorization Act of 2018 §346(b.2.C), 49 U.S.C. §44806

In this chart, the Class E airspace is bounded by a vignette magenta border, and spans down to 700 ft; anything below that is Class G airspace, and thus open for [UAV](#) operations. Incidentally, the area of payload operations lies beyond a 5 mile radius of the closest airfield.

2.1.2 Team-derived requirements

In addition to the above, a number of additional requirements have been compiled by the team. In particular, the robustness of the securement system, as well as the reliability of the deployment system are at the center of the discussion.



2.2 Means of Securement

2.3 Means of Deployment

2.4 Leading Design

Chapter 3

Operational Protocols

Throughout the mission, the **UAV** will encounter a number of varied tasks that must be completed sequentially so as to satisfy the mission objectives. As such, it is natural to define a number of regimes in which the vehicle must operate, as these dictate the operational protocols that are to be effectuated. This chapter details these operational regimes, including the pertinent operational protocols. Specifically, the following regimes are identified and discussed in due detail:

- I. Transit & Deployment
- II. Descent
- III. Loiter
- IV. Landing
- V. Retrieval

3.1 Transit & Deployment

Throughout stand-by, launch and passive descent, referred to as 'transit', the **UAV** will assume a low-power mode, periodically sending status updates and seeking connection with a ground station. This passive mode stems from multiple considerations. First, given the limited power supply, as much power as possible is to be saved will still maintaining a connection with the **UAV**. Second, by **FAA** regulations, the **UAV** may only be operated below 400 ft in **LOS**¹ [2]. To ensure that no active operation takes place above this ceiling, the vehicle will restrict its operations by considering its current altimeter reading as a locking mechanism. This 'altitude lock' constitutes the transit phase.

From the **FAA Reauthorization Act of 2018**, the following pertinent regulations may be found. The **UAV** must have a gross weight under 4.4 lbm, and must be operated:

- (i) within or beyond visual **LOS** of the operator;
- (ii) less than 400 ft above ground;
- (iii) during daylight conditions;
- (iv) within Class G airspace; and
- (v) outside of 5 statute miles from any airport, heliport, seaplane base, spaceport, or other location with aviation activities.

¹FAA Reauthorization Act of 2018 §346(b.2.C), 49 U.S.C. §44806

Regarding points (iv) and (v), it is found that the closest airport is the Hazel Green airport. However, the launch site, Bragg Farms, is located outside of the Class E airspace, thus respecting the Class G airspace requirement.

Given the fact that the payload will only be deployed upon being granted permission from the RSO, it is of importance to achieve a timely response in the event of late notification. In addition, proper coordination with the avionics systems is of importance, as solenoid disengagement and winch lowering must be followed by UAV arm deployment in close succession.

3.2 Descent

HE
Expand on deployment requirements (robustness, rapidity) and ground proximity considerations

3.3 Loiter

HE
Expand on descent phase, including trade-offs between guidance algorithms ((N)MPC, GPC) and waypoint tracking vs. visual guidance at close proximity (CV).

3.4 Landing

HE
Expand on loiter phase, highlighting energy efficiency and data acquisition (feature detection and path planning) during idle phase. Also detail what safety features must be incorporated into this phase (geofencing, no-fly zones have to default back to loiter).

3.5 Retrieval

HE
Expand on final approach and landing phase, including close-quarters operations and the role of computer vision in detecting the landing site, as well as the accuracy and terminal touch down conditions (velocity, attitude). Explain touch-and-go maneuvers in case of failed landing attempt.

HE
Expand on retrieval protocol, including claw operations and validation of claw contents. Explain the details on distancing and claw placement.

Chapter 4

Quadrotor Dynamic Model

4.1 Coordinate Systems

Let us consider the following four coordinate systems: (i) inertial, (ii) Earth-fixed, (iii) instantaneous topocentric, and (iv) body-fixed [3, pp. 3f.]. For these systems, the axes are defined as follows:

Inertial system (O at Earth center)

- X** On the Earth equatorial plane, pointing to the zero longitude at take-off
- Y** On the Earth equatorial plane, pointing to the 90° longitude at take-off
- Z** Perpendicular to the equatorial plane, pointing to the North Pole

Earth-fixed system (O_E at Earth center)

- X_E** On the Earth equatorial plane, always pointing to the Greenwich (0°) longitude
- Y_E** On the Earth equatorial plane, always pointing to the 90° longitude
- Z_E** Perpendicular to the equatorial plane, pointing to the North Pole

Instantaneous topocentric system (O_T at the projection point of the moving UAV on the Earth surface)

- x_T** On the local horizon plane tangent to the instantaneous projection point of the UAV, directed along the local geocentric North
- y_T** On the local horizon plane tangent to the instantaneous projection point of the UAV, directed along the local geocentric North
- z_T** Perpendicular to the instantaneous tangent plane, directed along the geocentric radius vector and pointing toward the Earth center

Body-fixed system (O_B at the center of gravity of the UAV)

- x_B** Along the UAV principle (longitudinal) axis, positive forward
- y_B** Normal to the x_B - z_B symmetric plane, completing the right-hand system
- z_B** In the principle plane of symmetry of the UAV, perpendicular to the x_B axis and positive downward

We will chiefly confine our discussion to the O_T (instantaneous topocentric system) and O_B (body-fixed) frames, as the distances the vehicle will travel allow for a flat Earth approximation with constant uniform gravity [4]. Let us now consider the coordinate transformation between these two frames:

4.1.1 Coordinate Transformation

Let us define the following Euler angles:

- θ Pitch
- ψ Yaw
- ϕ Roll

We then find the transformation from the instantaneous topocentric frame to the body-centric frame to be [5, Eq. 2-2]:

$$\begin{aligned} [R]_{T \rightarrow B}(\theta, \psi, \phi) &= \begin{bmatrix} 1 & 0 & 0 \\ 0 & \cos \phi & \sin \phi \\ 0 & -\sin \phi & \cos \phi \end{bmatrix} \begin{bmatrix} \cos \theta & 0 & -\sin \theta \\ 0 & 1 & 0 \\ \sin \theta & 0 & \cos \theta \end{bmatrix} \begin{bmatrix} \cos \psi & \sin \psi & 0 \\ -\sin \psi & \cos \psi & 0 \\ 0 & 0 & 1 \end{bmatrix} \\ &= \begin{bmatrix} \cos \theta \cos \psi & \cos \theta \sin \psi & -\sin \theta \\ \sin \theta \cos \psi \sin \phi - \sin \psi \cos \phi & \sin \theta \sin \psi \sin \phi + \cos \psi \cos \phi & \cos \theta \sin \phi \\ \sin \theta \cos \psi \cos \phi + \sin \psi \sin \phi & \sin \theta \sin \psi \cos \phi - \cos \psi \sin \phi & \cos \theta \cos \phi \end{bmatrix} \end{aligned} \quad (4.1.1)$$

Given the nature of the transformation matrix, it is readily found that:

$$[R]_{B \rightarrow T} = [R]_{T \rightarrow B}^{-1} = [R]_{T \rightarrow B}^{\top} \quad (4.1.2)$$

4.2 Dynamic Model

Given the complex nature of the rotor-based UAV, we will make the following a priori assumptions to aid in the derivation of the vehicle model:

1. The UAV is a rigid body.
2. The Tensor of Inertia (ToI) of the UAV is approximated as the Moment of Inertia (MoI) of several objects.
3. The Center of Mass (CM) coincides with the UAV's geometrical centroid.
4. The MoI of the propellers is neglected.
5. Time delay of commands is neglected.
6. Aerodynamic drag force is neglected.

While most of the aforestated simplifications are intuitively sound, neglecting the aerodynamic drag force begs for justification. Castillo et al. [6] provide the following approximation to the UAV drag force:

$$\mathbf{f}_{d_k} = C_{D_k} \rho A_k V_k (V_{w_k} - V_k) \hat{\mathbf{k}}, \quad k : x_b, y_b, z_b \quad (4.2.1)$$

Where $\hat{\mathbf{k}}$ is the unit vector in \mathbf{k} direction, A_k is the reference area by which the drag coefficient C_{D_k} is determined in the \mathbf{k} -direction. V_k and V_{w_k} are the vehicle velocity and wind velocity in O_B , respectively, and ρ is

the air density, which is assumed to be constant. In this formulation, C_{D_k} is to be determined through simulation ([Computational Fluid Dynamics \(CFD\)](#)) or experiment. However, this poses a significant difficulty: the [UAV](#) consists of many distinct components with orientation and speed dependent drag characteristics, making the definition of a constant C_{D_k} inadvisable. As a matter of fact, Castillo et al. [6] treat the drag force as an unknown disturbance that is to be counteracted by the control system, thus warranting the term to be dropped.

Let us define \mathbf{T} and \mathbf{H} , the thrust force and hub torque for every motor-propeller system, respectively. Research shows that these forces scale with the square of the angular rate of the propellor [5–9], i.e.:

$$T_i = k_T \omega_i^2 \quad (4.2.2)$$

$$H_i = k_H \omega_i^2 \quad (4.2.3)$$

where i denotes the i 'th propeller, and we assume the propellers to be identical, yielding constant k_T, k_H . These coefficients can be found experimentally. Following the Newton–Euler approach presented by Kurak and Hodzic [5], we find for a symmetric four-propeller [UAV](#) layout:

$$\ddot{\phi} = \frac{\ell(T_2 - T_4) - (I_z - I_y)\dot{\theta}\dot{\psi}}{I_x} \quad (4.2.4)$$

$$\ddot{\theta} = \frac{\ell(T_3 - T_1) - (I_x - I_z)\dot{\phi}\dot{\psi}}{I_y} \quad (4.2.5)$$

$$\ddot{\psi} = \frac{(H_1 + H_3) - (H_2 + H_4) - (I_y - I_x)\dot{\phi}\dot{\theta}}{I_z} \quad (4.2.6)$$

$$\ddot{x} = \frac{(\cos \phi \sin \theta \cos \psi + \sin \phi \sin \psi) \sum_{i=1}^4 T_i}{m} \quad (4.2.7)$$

$$\ddot{y} = \frac{(\cos \phi \sin \theta \sin \psi - \sin \phi \cos \psi) \sum_{i=1}^4 T_i}{m} \quad (4.2.8)$$

$$\ddot{z} = \frac{(\cos \phi \cos \theta) \sum_{i=1}^4 T_i - mg}{m} \quad (4.2.9)$$

where $I_k = I_{kk}, k : x, y, z$ are the diagonal elements of the [Tol I](#), ℓ is the L_2 -distance between the propeller and the origin of the O_B -frame (ℓ is constant to satisfy symmetry).

4.2.1 Nonlinear state space model

Let us define the following state variable:

$$\mathbf{x} = \begin{bmatrix} \phi \\ \dot{\phi} \\ \theta \\ \dot{\theta} \\ \psi \\ \dot{\psi} \\ z \\ \dot{z} \\ x \\ \dot{x} \\ y \\ \dot{y} \end{bmatrix} = \begin{bmatrix} x_1 \\ x_2 = \dot{x}_1 \\ x_3 \\ x_4 = \dot{x}_3 \\ x_5 \\ x_6 = \dot{x}_5 \\ x_7 \\ x_8 = \dot{x}_7 \\ x_9 \\ x_{10} = \dot{x}_9 \\ x_{11} \\ x_{12} = \dot{x}_{11} \end{bmatrix} \quad (4.2.10)$$

The force control input is then defined as:

$$\mathbf{u}^* = \begin{bmatrix} \sum_{i=1}^4 T_i \\ T_2 - T_4 \\ T_3 - T_1 \\ (H_1 + H_3) - (H_2 + H_4) \end{bmatrix} \quad (4.2.11)$$

Defining the angular rate control input as:

$$\mathbf{u} = \begin{bmatrix} \omega_1^2 \\ \omega_2^2 \\ \omega_3^2 \\ \omega_4^2 \end{bmatrix} \quad (4.2.12)$$

Using this definition, we find the force control input \mathbf{u}^* to be related to the angular rate control input \mathbf{u} as follows:

$$\mathbf{u}^* = \begin{bmatrix} k_T & k_T & k_T & k_T \\ 0 & k_T & 0 & -k_T \\ -k_T & 0 & k_T & 0 \\ k_H & -k_H & k_H & -k_H \end{bmatrix} \mathbf{u} \quad (4.2.13)$$

Let us now define the following constants:

$$a_1 = \frac{I_y - I_z}{I_x} \quad a_2 = \frac{I_z - I_x}{I_y} \quad a_3 = \frac{I_x - I_y}{I_z} \quad (4.2.14)$$

$$b_1 = \frac{\ell}{I_x} \quad b_2 = \frac{\ell}{I_y} \quad b_3 = \frac{\ell}{I_3} \quad (4.2.15)$$

and the following rotations:

$$\begin{aligned} r_t &= \cos \phi \cos \theta \\ r_x &= \cos \phi \sin \theta \cos \psi + \sin \phi \sin \psi \\ r_y &= \cos \phi \sin \theta \sin \psi - \sin \phi \cos \psi \end{aligned} \quad (4.2.16)$$

The nonlinear state space formulation is then found to be:

$$\dot{\mathbf{x}} = \begin{bmatrix} x_2 \\ x_4 x_6 a_1 + b_1 u_2^* \\ x_4 \\ x_2 x_6 a_2 + b_2 u_3^* \\ x_6 \\ x_2 x_4 a_3 + b_3 u_4^* \\ x_8 \\ -g + r_t(x_1, x_3) u_1^* / m \\ x_{10} \\ r_x(x_1, x_3, x_5) u_1^* / m \\ x_{12} \\ r_y(x_1, x_3, x_5) u_1^* / m \end{bmatrix} \quad (4.2.17)$$

4.2.2 Linearized state space model

Let us apply a small angle approximation on Eq. 4.2.16, giving:

$$\begin{aligned} r_t &\approx 1 \\ r_x &\approx \theta \\ r_y &\approx \theta\psi - \phi \approx -\phi \end{aligned} \quad (4.2.18)$$

To linearize Eq. 4.2.17, we must find a suitable equilibrium point, where $\dot{\mathbf{x}} = \mathbf{0}$. This holds for:

$$\begin{aligned} \bar{\mathbf{x}} &= \begin{bmatrix} 0 & 0 & 0 & 0 & 0 & 0 & \bar{x}_7 & 0 & \bar{x}_9 & 0 & \bar{x}_{11} \end{bmatrix}^\top \\ \bar{\mathbf{u}}^* &= \begin{bmatrix} mg & 0 & 0 & 0 \end{bmatrix}^\top \end{aligned} \quad (4.2.19)$$

Linearizing Eq. 4.2.17 about $(\bar{\mathbf{x}}, \bar{\mathbf{u}}^*)$, we obtain:

$$\begin{aligned} \mathbf{A} &= \left. \frac{\partial \dot{\mathbf{x}}(\mathbf{x}, \mathbf{u}^*)}{\partial \mathbf{x}} \right|_{(\bar{\mathbf{x}}, \bar{\mathbf{u}}^*)} \\ \mathbf{B} &= \left. \frac{\partial \dot{\mathbf{x}}(\mathbf{x}, \mathbf{u}^*)}{\partial \mathbf{u}^*} \right|_{(\bar{\mathbf{x}}, \bar{\mathbf{u}}^*)} \end{aligned} \quad (4.2.20)$$

which yields the following state space formulation:

$$\begin{aligned}
 \dot{\mathbf{x}} &= \underbrace{\begin{bmatrix} 0 & 1 & 0 & 0 & 0 & 0 & 0 & 0 & 0 & 0 & 0 & 0 \\ 0 & 0 & 0 & 0 & 0 & 0 & 0 & 0 & 0 & 0 & 0 & 0 \\ 0 & 0 & 0 & 1 & 0 & 0 & 0 & 0 & 0 & 0 & 0 & 0 \\ 0 & 0 & 0 & 0 & 0 & 0 & 0 & 0 & 0 & 0 & 0 & 0 \\ 0 & 0 & 0 & 0 & 0 & 0 & 1 & 0 & 0 & 0 & 0 & 0 \\ 0 & 0 & 0 & 0 & 0 & 0 & 0 & 0 & 0 & 0 & 0 & 0 \\ 0 & 0 & 0 & 0 & 0 & 0 & 0 & 0 & 0 & 0 & 0 & 0 \\ 0 & 0 & 0 & 0 & 0 & 0 & 0 & 1 & 0 & 0 & 0 & 0 \\ 0 & 0 & 0 & 0 & 0 & 0 & 0 & 0 & 0 & 0 & 0 & 0 \\ 0 & 0 & 0 & 0 & 0 & 0 & 0 & 0 & 0 & 0 & 1 & 0 \\ 0 & g & 0 & 0 & 0 & 0 & 0 & 0 & 0 & 0 & 0 & 0 \\ -g & 0 & 0 & 0 & 0 & 0 & 0 & 0 & 0 & 0 & 0 & 0 \end{bmatrix}}_{\mathbf{A}} \mathbf{x} + \underbrace{\begin{bmatrix} 0 & 0 & 0 & 0 \\ 0 & b_1 & 0 & 0 \\ 0 & 0 & 0 & 0 \\ 0 & 0 & b_2 & 0 \\ 0 & 0 & 0 & 0 \\ 0 & 0 & 0 & b_3 \\ 0 & 0 & 0 & 0 \\ 1/m & 0 & 0 & 0 \\ 0 & 0 & 0 & 0 \\ 0 & 0 & 0 & 0 \\ 0 & 0 & 0 & 0 \\ 0 & 0 & 0 & 0 \end{bmatrix}}_{\mathbf{B}^*} \mathbf{u}^* \\
 &= \mathbf{Ax} + \underbrace{\begin{bmatrix} 0 & 0 & 0 & 0 \\ 0 & b_1 k_T & 0 & -b_1 k_T \\ 0 & 0 & 0 & 0 \\ -b_2 k_T & 0 & b_2 k_T & 0 \\ 0 & 0 & 0 & 0 \\ b_3 k_H & -b_3 k_H & b_3 k_H & -b_3 k_H \\ 0 & 0 & 0 & 0 \\ \frac{k_T}{m} & \frac{k_T}{m} & \frac{k_T}{m} & \frac{k_T}{m} \\ 0 & 0 & 0 & 0 \\ 0 & 0 & 0 & 0 \\ 0 & 0 & 0 & 0 \end{bmatrix}}_{\mathbf{B}} \mathbf{u}
 \end{aligned} \tag{4.2.21}$$

4.2.3 Discretization

Zero-order Hold (ZOH) discretization of Eq. 4.2.21, gives for constant sampling time h :

$$\Phi = e^{Ah} = \begin{bmatrix} 1 & h & 0 & 0 & 0 & 0 & 0 & 0 & 0 & 0 & 0 & 0 \\ 0 & 1 & 0 & 0 & 0 & 0 & 0 & 0 & 0 & 0 & 0 & 0 \\ 0 & 0 & 1 & h & 0 & 0 & 0 & 0 & 0 & 0 & 0 & 0 \\ 0 & 0 & 0 & 1 & 0 & 0 & 0 & 0 & 0 & 0 & 0 & 0 \\ 0 & 0 & 0 & 0 & 1 & h & 0 & 0 & 0 & 0 & 0 & 0 \\ 0 & 0 & 0 & 0 & 0 & 1 & h & 0 & 0 & 0 & 0 & 0 \\ 0 & 0 & 0 & 0 & 0 & 0 & 1 & 0 & 0 & 0 & 0 & 0 \\ 0 & 0 & 0 & 0 & 0 & 0 & 0 & 1 & h & 0 & 0 & 0 \\ 0 & \frac{gh^2}{2} & 0 & 0 & 0 & 0 & 0 & 0 & 1 & h & 0 & 0 \\ 0 & gh & 0 & 0 & 0 & 0 & 0 & 0 & 0 & 1 & 0 & 0 \\ -\frac{gh^2}{2} & -\frac{gh^3}{6} & 0 & 0 & 0 & 0 & 0 & 0 & 0 & 0 & 1 & h \\ -gh & -\frac{gh^2}{2} & 0 & 0 & 0 & 0 & 0 & 0 & 0 & 0 & 0 & 1 \end{bmatrix} \quad (4.2.22)$$

$$\Gamma = \int_0^h e^{As} ds \cdot \mathbf{B} = \begin{bmatrix} 0 & \frac{1}{2}b_1h^2k_T & 0 & -\frac{1}{2}b_1h^2k_T \\ 0 & b_1hk_T & 0 & b_1(-h)k_T \\ -\frac{1}{2}b_2h^2k_T & 0 & \frac{1}{2}b_2h^2k_T & 0 \\ b_2(-h)k_T & 0 & b_2hk_T & 0 \\ \frac{1}{2}b_3h^2k_H & -\frac{1}{2}b_3h^2k_H & \frac{1}{2}b_3h^2k_H & -\frac{1}{2}b_3h^2k_H \\ b_3hk_H & b_3(-h)k_H & b_3hk_H & b_3(-h)k_H \\ \frac{h^2k_T}{h^2k_T} & \frac{h^2k_T}{h^2k_T} & \frac{h^2k_T}{h^2k_T} & \frac{h^2k_T}{h^2k_T} \\ \frac{h^2k_T}{h^2k_T} & \frac{h^2k_T}{h^2k_T} & \frac{h^2k_T}{h^2k_T} & \frac{h^2k_T}{h^2k_T} \\ m & m & m & m \\ 0 & \frac{1}{6}b_1gh^3k_T & 0 & -\frac{1}{6}b_1gh^3k_T \\ 0 & \frac{1}{2}b_1gh^2k_T & 0 & -\frac{1}{2}b_1gh^2k_T \\ 0 & -\frac{1}{24}b_1gh^4k_T & 0 & \frac{1}{24}b_1gh^4k_T \\ 0 & -\frac{1}{6}b_1gh^3k_T & 0 & \frac{1}{6}b_1gh^3k_T \end{bmatrix} \quad (4.2.23)$$

with the following state space system:

$$\mathbf{x}(k+1) = \Phi\mathbf{x}(k) + \Gamma\mathbf{u}(k) \quad (4.2.23)$$

4.3 Simulation

From Tayebi and McGilvray [10], we adopt the following values for our simulation:

Table 4.1: Simulation parameters [10]

Parameter	Value
g	9.81 m s^{-2}
m	0.468 kg
ℓ	0.225 m
k_T	$2.980 \times 10^{-6} (\text{rad}^2/\text{s}^2)/\text{N}$
k_H	$1.140 \times 10^{-7} (\text{rad}^2/\text{s}^2)/\text{Nm}$
I_x	$4.856 \times 10^{-3} \text{ kg m}^{-2}$
I_y	$4.856 \times 10^{-3} \text{ kg m}^{-2}$
I_z	$8.801 \times 10^{-3} \text{ kg m}^{-2}$

Letting $h = 1 \times 10^{-3} \text{ s}$, we obtain:

$$\Phi = \begin{bmatrix} 1 & 0.001 & 0 & 0 & 0 & 0 & 0 & 0 & 0 & 0 & 0 \\ 0 & 1 & 0 & 0 & 0 & 0 & 0 & 0 & 0 & 0 & 0 \\ 0 & 0 & 1 & 0.001 & 0 & 0 & 0 & 0 & 0 & 0 & 0 \\ 0 & 0 & 0 & 1 & 0 & 0 & 0 & 0 & 0 & 0 & 0 \\ 0 & 0 & 0 & 0 & 1 & 0.001 & 0 & 0 & 0 & 0 & 0 \\ 0 & 0 & 0 & 0 & 0 & 1 & 0 & 0 & 0 & 0 & 0 \\ 0 & 0 & 0 & 0 & 0 & 0 & 1 & 0.001 & 0 & 0 & 0 \\ 0 & 0 & 0 & 0 & 0 & 0 & 0 & 1 & 0 & 0 & 0 \\ 0 & 4.905 \times 10^{-6} & 0 & 0 & 0 & 0 & 0 & 0 & 1 & 0.001 & 0 \\ 0 & 0.00981 & 0 & 0 & 0 & 0 & 0 & 0 & 0 & 1 & 0 \\ -4.905 \times 10^{-6} & -1.635 \times 10^{-9} & 0 & 0 & 0 & 0 & 0 & 0 & 0 & 0 & 1 \\ -0.00981 & -4.905 \times 10^{-6} & 0 & 0 & 0 & 0 & 0 & 0 & 0 & 0 & 1 \end{bmatrix} \quad (4.3.1)$$

$$\Gamma = \begin{bmatrix} 1 & 0.001 & 0 & 0 & 0 & 0 & 0 & 0 & 0 & 0 & 0 \\ 0 & 1 & 0 & 0 & 0 & 0 & 0 & 0 & 0 & 0 & 0 \\ 0 & 0 & 1 & 0.001 & 0 & 0 & 0 & 0 & 0 & 0 & 0 \\ 0 & 0 & 0 & 1 & 0 & 0 & 0 & 0 & 0 & 0 & 0 \\ 0 & 0 & 0 & 0 & 1 & 0.001 & 0 & 0 & 0 & 0 & 0 \\ 0 & 0 & 0 & 0 & 0 & 1 & 0 & 0 & 0 & 0 & 0 \\ 0 & 0 & 0 & 0 & 0 & 0 & 1 & 0.001 & 0 & 0 & 0 \\ 0 & 4.905 \times 10^{-6} & 0 & 0 & 0 & 0 & 0 & 0 & 1 & 0.001 & 0 \\ 0 & 0.00981 & 0 & 0 & 0 & 0 & 0 & 0 & 0 & 1 & 0 \\ -4.905 \times 10^{-6} & -1.635 \times 10^{-9} & 0 & 0 & 0 & 0 & 0 & 0 & 0 & 0 & 1 \\ -0.00981 & -4.905 \times 10^{-6} & 0 & 0 & 0 & 0 & 0 & 0 & 0 & 0 & 1 \end{bmatrix}$$

4.4 Controller Design

This section details the controller setup and design for the UAV. We concern ourselves chiefly with the servo problem, with path generation being delegated to the guidance law. Given the nature of the problem, we are

forced to employ the [LQR](#) methodology to tune the gains for this [Multiple Input Multiple Output \(MIMO\)](#) system.

4.4.1 LQR Tuning

Following the guidelines from [11], we are to work with the following cost function:

$$\mathcal{J} = \rho \mathbf{x}^\top \mathbf{H}_w^\top \bar{\mathbf{Q}}_1 \mathbf{H}_w \mathbf{x} + \mathbf{u}^\top \mathbf{Q}_2 \mathbf{u} \quad (4.4.1)$$

where \mathbf{Q} is a diagonal matrix containing elements that equal the inverse of the square of the maximum deviation of the states/inputs of interest. The value of ρ is to be tuned by trial and error, considering the properties of the response.

State weighting matrix. Since we wish to have full state control with minimal deviations on every state, we will pose $\mathbf{H}_w = \mathbf{I}_{12}$. Given this choice of \mathbf{H}_w , we find $\bar{\mathbf{Q}}_1 = \mathbf{Q}_1$. We find $\bar{\mathbf{Q}}_1$ to be of the form:

$$\bar{\mathbf{Q}}_1 = \begin{bmatrix} \Delta x_1^{-2} & 0 & \dots & 0 \\ 0 & \Delta x_2^{-2} & \ddots & \vdots \\ \vdots & \ddots & \ddots & 0 \\ 0 & \dots & 0 & \Delta x_{12}^{-2} \end{bmatrix} \quad (4.4.2)$$

where the entries are tabulated in Tab. 4.2. The rationale behind the magnitude of these bounds lies in the mission objective of the [UAV](#); we wish to accomplish minute maneuvering and near-stationary hovering with closely matching attitude and small slew rate. As can be seen from the values, we place a greater importance on the vertical (z -axis) motion, such that the vehicle can accomplish accurate terrain following and close-quarters operations close to the surface.

Table 4.2: Maximum state deviation values for use in the $\bar{\mathbf{Q}}_1$ matrix in the [LQR](#) routine

State	Variable	Maximum state deviation
Δx_1	ϕ	$2.5^\circ \approx 4.36 \times 10^{-2} \text{ rad}$
Δx_2	$\dot{\phi}$	$1.25^\circ \text{ s}^{-1} \approx 2.18 \times 10^{-2} \text{ rad s}^{-1}$
Δx_3	θ	$2.5^\circ \approx 4.36 \times 10^{-2} \text{ rad}$
Δx_4	$\dot{\theta}$	$1.25^\circ \text{ s}^{-1} \approx 2.18 \times 10^{-2} \text{ rad s}^{-1}$
Δx_5	ψ	$5^\circ \approx 8.73 \times 10^{-2} \text{ rad}$
Δx_6	$\dot{\psi}$	$2.5^\circ \text{ s}^{-1} \approx 4.36 \times 10^{-2} \text{ rad s}^{-1}$
Δx_7	z	0.025 m
Δx_8	\dot{z}	0.0125 m s^{-1}
Δx_9	x	0.05 m
Δx_{10}	\dot{x}	0.025 m s^{-1}
Δx_{11}	y	0.05 m
Δx_{12}	\dot{y}	0.025 m s^{-1}

Control weighting matrix. For the control input, we wish to minimize the use of excessive throttle. We can accomplish this by setting $\Delta u_i = 2^{-1/2} \omega_{\max}^2$ for $i \in [1, 4]$. This will translate to a maximum of $\pm 71\%$ throttle on each rotor, yielding a thrust cap at the [Root Mean Square \(RMS\)](#) value of the maximum thrust,

$T_{\text{cap}} = T_{\text{max}}/\sqrt{2}$, if we assume it to vary as a sinusoid. Similar to the state weighting matrix, the control weighting matrix will assume the form of:

$$\begin{bmatrix} \Delta u_1^{-2} & 0 & \dots & 0 \\ 0 & \Delta u_2^{-2} & \ddots & \vdots \\ \vdots & \ddots & \ddots & 0 \\ 0 & \dots & 0 & \Delta u_4^{-2} \end{bmatrix} \quad (4.4.3)$$

Summarizing, we obtain the following cost function:

$$\mathcal{J} = \rho \mathbf{x}^\top \mathbf{Q} \mathbf{x} + \mathbf{u}^\top \mathbf{Q}_2 \mathbf{u} \quad (4.4.4)$$

Part V

Safety

Chapter 5

Safety Plan Overview

The safety of all team members is of the absolute highest priority for the Illinois Space Society Student Launch team. Should a situation arise in which a project-critical choice needs to be made, safety is considered before the success of the project. The safety officer this year is Zana Essmyer, who is overseeing a small team to conduct a thorough analysis of any hazards the team may encounter this year throughout the design, construction, assembly, and launches of the rocket and payload. Zana and the safety team are also implementing plans and procedures to minimize the risk of associated hazards.

This year, using a combination of in-person briefings, online classes and thorough documentation, the team is actively encouraging participation in the adherence to safety procedures. Safety training is required for any member that wishes to participate in construction sessions or attend a launch. By keeping lists of safety-trained members and having experienced members actively involved at every build session, the team can ensure that everyone working in lab spaces understands safety protocol for both day-to-day work and potential emergency situations. Forthcoming checklists will also be developed to ensure total safety during the off-pad, on-pad and post flight procedures.

5.1 Emergency Preparedness

Though the Illinois Space Society strives to maintain a safe working environment during all phases of the competition, the team also recognizes that accidents remain a possibility even with the strictest safety precautions in place. With this in mind, emergency preparedness forms another pillar of the team's safety plan. First aid kits are easily accessible in all of the team's main workspaces, and the safety officer has familiarized herself with their contents. The kits themselves are up-to-date and include wound dressings, antibiotic ointments, painkillers, and antihistamines. For any injuries requiring more than basic first aid, medical facilities are available both on and off the University of Illinois campus.

5.2 Incident Reporting

In the rare event that an accident requiring first aid occurs, the primary goal is always to care for and assist the injured team member. That said, once the incident has passed, the safety team's next priority is to actively prevent accident reoccurrence. Any incident is to be reported immediately to the safety officer, and from there it will be her responsibility to speak to those involved and determine the exact cause of the accident. Review of an incident will be considered complete once the safety officer has surveyed the scenario to her satisfaction and offered recommendations to the team leadership on how to prevent similar incidents in the future.

If an incident happens to occur, a series of actions will enact. The non-injured team member will assess the situation for any immediate dangers before contacting the Safety Officer, Technical Manager, and, if needed, emergency personnel. The Safety Officer will document the incident. The safety team will then take action to prevent further incidents.

5.3 Equipment Training

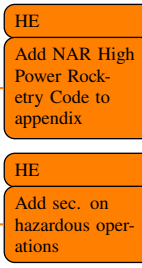
In order to provide team members with the experience necessary to operate a wide array of equipment and tooling, the safety team provides tutorial sessions on all machinery and tooling that may be used during the course of construction that is provided in the Nuclear Engineering Laboratory. To that end, the safety team has duplicated or adapted manufacturer-provided operating procedures for these tools and uploaded them to the team's shared drive for easy access. A collection of all training documents can be found in APPENDIX D: ISS Common Materials and Equipment Training with information included for the following devices:

- Full Spectrum Laser Professional Series CO2 48"×36" Cutter
- Ultimaker 2 Extended 3D Printer
- Milwaukee Sawzall Reciprocating Saw
- DeWalt 18V Wireless Power Drill
- Dremel 8200-1/28 12-Volt Max Cordless Rotary Tool
- G5000 RocketPoxy
- Grizzly Model G7297 12" Disc Sander
- Water-Cooled Diamond Table Saw
- Grizzly H2936 Vacuum Sanding Table
- GMC 16" Scroll Saw
- JET 15" Bench Drill Press
- Soldering Station
- Miscellaneous Hand Tools (Screwdrivers, Hammer, Clamps, etc.)

In order to operate this machinery, a team member must attend tutorial sessions or receive training separately from a member of the safety team or team management. In providing and requiring these sessions, the team not only reduces the risk of mishaps due to misuse of equipment, but also ensures redundancy in knowledge of construction techniques. The Safety Officer will host tutorial sessions for ESPL machinery at the beginning of the semester for all members before access will be granted.

5.4 NAR/TRA Procedures

The team will comply with the “High Power Rocket Safety Code” provided on the NAR website that has been effective since August 2012. The 13-step code and Minimum Distance Table on the website will be reviewed by the safety officer. All members on the team will be required to read the safety code online as it is a relatively short list of codes. The rules set forth by the NAR High Power Rocketry Code will always be respected and followed as they are set to ensure the safety of people and the environment. The safety officer, team manager, and sub-team managers will always make sure to comply with the safety code and ensure the rest of the team is properly complying. A copy of the NAR High Power Rocketry Code is included in this report as . Additionally, sections and elaborate on the hazardous operations and mitigation of risks. Hazardous materials and proper protocol is detailed under section.



NAR Mentor. Mark Joseph will be the NAR mentor for the ISS Student Launch team for this year’s competition. In addition to his longtime involvement in the high-power rocketry community, Mark has worked with the ISS team for several years now in the NASA Space Grant, Intercollegiate Rocket Engineering, and Student Launch Competitions.

Chapter 6

Risk Assessment Overview

To better prepare for issues that inevitably arise during any project of large scale and to prioritize the team's time, the safety team has conducted a thorough risk analysis based on incident severity. The safety team analyzed risks to the project, the environment, and above all, the health of team members during the construction process. The team used Risk Assessment Codes (RACs) to evaluate the various hazards to both personnel and the project. Table 6.1 introduces the risk matrix and the risk assessment codes that will be used to classify risks throughout the rest of the safety section. Risks are color-coded based on their severity, and discusses the team's response to these various levels. defines the levels of severity as it relates to personnel, project, and environmental health. Table 9 defines individual instance probability and probability of occurrence throughout the entire project timeline.

Table 6.1: Level of risk and member requirements

Probability	Severity			
	1—Catastrophic	2—Critical	3—Marginal	4—Negligible
A—Frequent	1A	2A	3A	4A
B—Probable	1B	2B	3B	4B
C—Occasional	1C	2C	3C	4C
D—Remote	1D	2D	3D	4D
E—Improbable	1E	2E	3E	4E

Part VI

Project Plan

Bibliography

- [1] 2020 NASA Student Launch Handbook and Request for Proposal. Handbook, Office of STEM Engagement NASA Marshall Space Flight Center, Huntsville, AL, August 2019.
- [2] Federal Aviation Administration. FAA Reauthorization Act of 2018, November 2018.
- [3] Raghubansh P. Singh, Louis C. P. Huang, and Roland A. Cook. SENS-5D Trajectory and Wind-Sensitivity Calculations for Unguided Rockets. Contractor Report, Computer Sciences Corporation, Wallops Island, VA, December 1975. Prepared under Contract No. NAS6-2369 for Wallops Flight Center, Wallops Island, VA.
- [4] Lior M. Burko and Richard H. Price. Ballistic trajectory: Parabola, ellipse, or what? *American Journal of Physics*, 73(6):516–520, June 2005. doi: 10.1119/1.1866097.
- [5] Sevkuthan Kurak and Migdat Hodzic. Control and Estimation of a Quadcopter Dynamical Model. *Periodicals of Engineering and Natural Sciences (PEN)*, 6(1):63, March 2018. ISSN 23034521. doi: 10.21533/pen.v6i1.164.
- [6] Pedro Castillo, Laura Elena Muñoz Hernández, and Pedro García Gil. *Indoor Navigation Strategies for Aerial Autonomous Systems*. Butterworth-Heinemann, Oxford, 2017. ISBN 978-0-12-805189-4. OCLC: ocn958449100.
- [7] Justin Winslow, Vikram Hrishikeshavan, and Inderjit Chopra. Design Methodology for Small-Scale Unmanned Quadrotors. *Journal of Aircraft*, 55(3):1062–1070, May 2018. ISSN 0021-8669, 1533-3868. doi: 10.2514/1.C034483.
- [8] Dmitry Bershadsky, Steve Haviland, and Eric N. Johnson. Electric Multirotor UAV Propulsion System Sizing for Performance Prediction and Design Optimization. In *57th AIAA/ASCE/AHS/ASC Structures, Structural Dynamics, and Materials Conference*, San Diego, California, USA, January 2016. American Institute of Aeronautics and Astronautics. ISBN 978-1-62410-392-6. doi: 10.2514/6.2016-0581.
- [9] Teppo Luukkonen. Modelling and control of quadcopter. Independent research, Aalto University, School of Science, Espoo, Finland, August 2011.
- [10] A. Tayebi and S. McGilvray. Attitude stabilization of a four-rotor aerial robot. In *2004 43rd IEEE Conference on Decision and Control (CDC) (IEEE Cat. No.04CH37601)*, pages 1216–1221 Vol.2, Nassau, Bahamas, 2004. IEEE. ISBN 978-0-7803-8682-2. doi: 10.1109/CDC.2004.1430207.
- [11] Gene F. Franklin, J. David Powell, and Michael L. Workman. *Digital Control of Dynamic Systems*. Addison-Wesley, Menlo Park, Calif., 3rd ed. edition, 2002. ISBN 978-0-201-82054-6 978-0-201-33153-0. OCLC: 249361424.